

# Critical coupling to Tamm plasmons

Baptiste Auguie\*, Axel Bruchhausen, Alejandro Fainstein

Centro Atómico Bariloche e Instituto Balseiro, San Carlos de Bariloche, 8400 Río Negro,  
Argentina

\*[baptiste.auguie@cab.cnea.gov.ar](mailto:baptiste.auguie@cab.cnea.gov.ar)

**Abstract:** The conditions of critical coupling of light to Tamm plasmons are investigated with comprehensive numerical simulations, highlighting the parameters that maximise absorption of incident light in the metal layer. The asymmetric response in reflection and absorption with respect to the direction of incidence is discussed, the two cases yielding different optimal coupling conditions. These findings are relevant for the design of optimised Tamm structures, particularly in applications such as narrow-band thermal emitters, field-enhanced spectroscopy and refractive-index sensing.

© 2014 Optical Society of America

**OCIS codes:** (310.3915) Metallic, opaque, and absorbing coatings; (250.5403) Plasmonics; (310.1620) Interference coatings; (260.5740) Resonance

---

## References and links

1. J. A. Gaspar-Armenta and F. Villa, "Photonic surface-wave excitation: photonic crystal-metal interface," *Journal of the Optical Society of America B* **20**, 2349–2354 (2003).
2. M. Kaliteevski, I. Iorsh, S. Brand, R. Abram, J. Chamberlain, A. Kavokin, and I. Shelykh, "Tamm plasmon-polaritons: Possible electromagnetic states at the interface of a metal and a dielectric Bragg mirror," *Phys. Rev. B* **76**, 165415 (2007).
3. M. Sasin, R. Seisyan, M. Kaliteevski, S. Brand, R. Abram, J. Chamberlain, I. Iorsh, I. Shelykh, A. Egorov, A. Vasil'ev, V. Mikhlin, and A. Kavokin, "Tamm plasmon-polaritons: First experimental observation," *Superlattices Microstruct.* **47**, 44–49 (2010).
4. C. Symonds, A. Lemaître, E. Homeyer, J. Plenat, and J. Bellessa, "Emission of Tamm plasmon/exciton polaritons," *Appl. Phys. Lett.* **95**, 151114 (2009).
5. K. Leosson, S. Shayestehaminzadeh, T. K. Tryggvason, A. Kossov, B. Agnarsson, F. Magnus, S. Olafsson, J. T. Gudmundsson, E. B. Magnusson, and I. A. Shelykh, "Comparing resonant photon tunneling via cavity modes and Tamm plasmon polariton modes in metal-coated Bragg mirrors," *Opt. Lett.* **37**, 4026–4028 (2012).
6. C. Symonds, A. Lemaître, P. Senellart, M. Jomaa, S. Aberra Guebrou, E. Homeyer, G. Brucoli, and J. Bellessa, "Lasing in a hybrid GaAs/silver Tamm structure," *Appl. Phys. Lett.* **100**, 121122 (2012).
7. X.-L. Zhang, J.-F. Song, X.-B. Li, J. Feng, and H.-B. Sun, "Light trapping schemes in organic solar cells: A comparison between optical Tamm states and Fabry-Pérot cavity modes," *Org. Electron.* **14**, 1577–1585 (2013).
8. C.-H. Xue, H.-T. Jiang, H. Lu, G.-Q. Du, and H. Chen, "Efficient third-harmonic generation based on Tamm plasmon polaritons," *Opt. Lett.* **38**, 959–961 (2013).
9. K. J. Lee, J. W. Wu, and K. Kim, "Enhanced nonlinear optical effects due to the excitation of optical Tamm plasmon polaritons in one-dimensional photonic crystal structures," *Opt. Express* **21**, 28817 (2013).
10. B. Afinogenov, V. Bessonov, and A. Fedyanin, "Giant second-harmonic generation enhancement in the presence of Tamm plasmon-polariton," in "Frontiers in Optics 2013," (Optical Society of America, 2013), p. FW5C.4.
11. B. Auguie, M. C. Fuertes, P. C. Angelomé, N. L. Abdala, G. J. A. A. Soler Illia, and A. Fainstein, "Tamm plasmon resonance in mesoporous multilayers: Toward a sensing application," *ACS Photonics* **1**, 775–780 (2014).
12. Y. Cui, Y. He, Y. Jin, F. Ding, L. Yang, Y. Ye, S. Zhong, Y. Lin, and S. He, "Plasmonic and metamaterial structures as electromagnetic absorbers," arXiv:1404.5695 (2014).
13. B. J. Lee, C. J. Fu, and Z. M. Zhang, "Coherent thermal emission from one-dimensional photonic crystals," *Applied Physics Letters* **87**, 071904 (2005).
14. K. Bliokh, Y. Bliokh, V. Freilikher, S. Savel'ev, and F. Nori, "Colloquium: Unusual resonators: Plasmonics, metamaterials, and random media," *Reviews of Modern Physics* **80**, 1201–1213 (2008).
15. S. Herminghaus, M. Klopffleisch, and H. J. Schmidt, "Attenuated total reflectance as a quantum interference phenomenon," *Optics Letters* **19**, 293–295 (1994).

16. B. Neuner III, D. Korobkin, C. Fietz, D. Carole, G. Ferro, and G. Shvets, "Critically coupled surface phonon-polariton excitation in silicon carbide," in "SPIE NanoScience+ Engineering," (International Society for Optics and Photonics, 2009), pp. 73942B–73942B.
17. J. R. Tischler, M. S. Bradley, and V. Bulović, "Critically coupled resonators in vertical geometry using a planar mirror and a 5 nm thick absorbing film," *Opt. Lett.* **31**, 2045–2047 (2006).
18. S. Y. Vetrov, R. G. Bikbaev, and I. V. Timofeev, "Optical Tamm states at the interface between a photonic crystal and a nanocomposite with resonance dispersion," *Journal of Experimental and Theoretical Physics* **117**, 988–998 (2013).
19. J. R. Piper and S. Fan, "Total absorption in a graphene monolayer in the optical regime by critical coupling with a photonic crystal guided resonance," *ACS Photonics* **1**, 347–353 (2014).
20. G.-q. Du, H.-t. Jiang, Z.-s. Wang, Y.-p. Yang, Z.-l. Wang, H.-q. Lin, and H. Chen, "Heterostructure-based optical absorbers," *J. Opt. Soc. Am. B* **27**, 1757–1762 (2010).
21. Y. Gong, X. Liu, H. Lu, L. Wang, and G. Wang, "Perfect absorber supported by optical Tamm states in plasmonic waveguide," *Optics Express* **19**, 18393–18398 (2011).
22. E. C. L. Ru and P. G. Etchegoin, *Principles of Surface Enhanced Raman Spectroscopy and Related Plasmonic Effects* (Elsevier, Amsterdam, 2009).
23. A. Amir and P. Vukusic, "Elucidating the stop bands of structurally colored systems through recursion," *American Journal of Physics* **81**, 253–257 (2013).
24. H. A. Haus, *Waves and fields in optoelectronics*, vol. Prentice-Hall Series in Solid State Physical Electronics (Englewood Cliffs, NJ, USA: Prentice Hall, 1978).
25. H. Macleod, *Thin-Film Optical Filters, Fourth Edition*, Series in Optics and Optoelectronics (Taylor & Francis, 2010).
26. M. Sasin, R. Seisyan, M. Kalitchevski, S. Brand, R. Abram, J. Chamberlain, A. Egorov, A. Vasil'Ev, V. Mikhlin, and A. Kavokin, "Tamm plasmon polaritons: Slow and spatially compact light," *Appl. Phys. Lett.* **92**, 251112 (2008).
27. S. Tsang, S. Yu, X. Li, H. Yang, and H. Liang, "Observation of Tamm plasmon polaritons in visible regime from ZnO/Al<sub>2</sub>O<sub>3</sub> distributed Bragg reflector – Ag interface," *Opt. Commun.* **284**, 1890–1892 (2011).
28. D. Zhang, Y. Chen, L. Zhu, Q. Fu, R. Wang, p. wang, H. Ming, J. R. Lakowicz, and R. Badugu, "Effect of metal film thickness on Tamm plasmon-coupled emission," *Phys. Chem. Chem. Phys.* (2014).
29. S. Brand, M. Kalitchevski, and R. Abram, "Optical Tamm states above the bulk plasma frequency at a Bragg stack/metal interface," *Phys. Rev. B* **79** (2009).
30. R. Badugu, E. Descrovi, and J. R. Lakowicz, "Radiative decay engineering 7: Tamm state-coupled emission using a hybrid plasmonic–photonic structure," *Anal. Biochem.* **445**, 1–13 (2014).
31. R. Badugu and J. R. Lakowicz, "Tamm state-coupled emission: Effect of probe location and emission wavelength," *The Journal of Physical Chemistry C* p. 140829102309004 (2014).
32. A. Tittl, M. G. Harats, R. Walter, X. Yin, M. Schäferling, N. Liu, R. Rapaport, and H. Giessen, "Quantitative angle-resolved small-spot reflectance measurements on plasmonic perfect absorbers: Impedance matching and disorder effects," *ACS Nano* (2014).
33. G. Du, L. Cui, L. Zhang, and H. Jiang, "Tamm plasmon polaritons in composite structures composed of the metal film and truncated photonic crystals," *Applied Physics A: Materials Science and Processing* **109**, 907–911 (2012).
34. S. A. Maier, *Plasmonics: Fundamentals and Applications* (Springer, 2007).
35. J. Homola, S. S. Yee, and G. Gauglitz, "Surface plasmon resonance sensors: review," *Sensors and actuators B* **54**, 3–15 (1999).
36. N. D. Lanzillotti-Kimura, A. Fainstein, A. Huynh, B. Perrin, B. Jusserand, A. Miard, and A. Lemaître, "Coherent generation of acoustic phonons in an optical microcavity," *Phys. Rev. Lett.* **99**, 217405 (2007).
37. A. Fainstein, N. D. Lanzillotti-Kimura, B. Jusserand, and B. Perrin, "Strong optical-mechanical coupling in a vertical GaAs/AlAs microcavity for subterahertz phonons and near-infrared light," *Phys. Rev. Lett.* **110**, 037403 (2013).

---

## 1. Introduction

Tamm plasmons (TP) are electromagnetic modes confined between a Distributed Bragg Reflector (DBR) and a noble metal (e.g. gold) [1–3]; in contrast to surface-plasmons they may be excited at normal incidence and present a relatively high quality factor, triggering interest as a convenient platform for enhanced light-matter interaction at the nanoscale [4–11]. Upon excitation of TPs with light, a dip in reflectivity is observed, which may reach 0% (critical coupling condition) for optimised structures, whereby optical energy is distributed between transmission and absorption channels. Many designs of plasmonic nanostructures have been proposed with the purpose of harnessing visible and infra-red light with greater efficiency [12]. Potential ap-

plications include solar cells, display and lighting technologies, optical sensors, and, by virtue of Kirchhoff’s law, thermal emitters [13]. The planar design of the Tamm structure, of great simplicity and amenable to large-scale fabrication, offers a clear advantage over more complex, 3-dimensional plasmonic nanostructures. This work aims to present a simple and accurate physical picture for optimising the coupling of incident light to TPs in realistic structures, supported by insights from the theory of critical coupling and extensive numerical simulations.

### 1.1. Critical coupling of light to open resonators

A Tamm structure may be regarded as a dissymmetric cavity, enclosed by a metal mirror on one side, and a DBR on the other. Based on the general theory of open resonators [14], resonant transmittance and reflectance take the form,

$$T = \frac{4\Gamma_{\text{rad}}^1\Gamma_{\text{rad}}^2}{(\Gamma_{\text{rad}}^1 + \Gamma_{\text{rad}}^2 + \Gamma_{\text{diss}})^2}, \quad R = \frac{(\Gamma_{\text{rad}}^2 - \Gamma_{\text{rad}}^1 + \Gamma_{\text{diss}})^2}{(\Gamma_{\text{rad}}^1 + \Gamma_{\text{rad}}^2 + \Gamma_{\text{diss}})^2} \quad (1)$$

where  $\Gamma_{\text{diss}}$  is the damping factor due to intrinsic (ohmic) loss,  $\Gamma_{\text{rad}}^1$  and  $\Gamma_{\text{rad}}^2$  the radiative loss factors for the two barriers. The transmittance  $T$  may reach unity only for non-absorbing, symmetric structures ( $\Gamma_{\text{diss}} = 0$ ,  $\Gamma_{\text{rad}}^1 = \Gamma_{\text{rad}}^2$ ). This situation occurs in dielectric cavities surrounded by two identical DBRs; in this case the response of the cavity improves monotonically with the reflectivity of the two mirrors. The quality factor increases with the number of layers, yielding a higher field enhancement inside the cavity, and maintaining complete transmission at resonance. The introduction of a lossy metallic element drastically changes the situation [14]. Unit transmission is no longer possible, as light undergoes absorption while interacting with the lossy structure. Reflection may still reach 0%, under the critical coupling condition  $\Gamma_{\text{diss}} = \Gamma_{\text{rad}}^1 - \Gamma_{\text{rad}}^2$ . When transmission is prohibited ( $\Gamma_{\text{rad}}^2 = 0$ ), e.g. by way of total internal reflection [15], critical coupling coincides with complete light absorption. The precise balance between radiative and non-radiative loss channels gives rise to a rich behaviour in the optical response, when varying the structural parameters and incidence conditions. Previous works have described complete absorption in similar planar multilayers; in fact original studies preceding what is now labelled a ‘‘Tamm plasmon’’ structure considered the related problem of maximising thermal emissivity in a DBR-absorber structure [16], supporting surface phonon-polaritons. Perfect light absorbers based on a DBR-lossy layer combination have also been proposed, using J-aggregates [17], nanoparticle composites [18], graphene [19], or metal films [20, 21]. However, to the best of our knowledge, no systematic review of the critical coupling mechanism with Tamm plasmons has been presented thus far. The present article aims to cover this topic; in particular we describe the conditions that yield vanishing reflectance for the Tamm structure, and further discriminate the regime of complete light absorption.

### 1.2. Review of the Tamm plasmon resonance

The Tamm structure is presented in Fig 1 (a). Although the discussion would equally apply to other materials and spectral range of operation, we will focus here on an experimentally-relevant configuration in the near-infrared region, using AIAs and GaAs for the DBR layers (refractive index  $n_L = 3.0$  and  $n_H = 3.7$ , respectively, and quarter-wave layer thickness for an operating wavelength of 950 nm), and the complex dielectric function for the gold layer obtained from Ref. [22]. We note that in this long-wavelength regime, away from the region of interband transitions, gold closely follows the behaviour of a free-electron metal and is also well described by a simple Drude model. To obtain the resonance condition associated with TPs, we take the pragmatic approach of looking for a pole in the complex reflectivity coefficient associated with the multilayer structure. We follow here a recursive treatment based on the

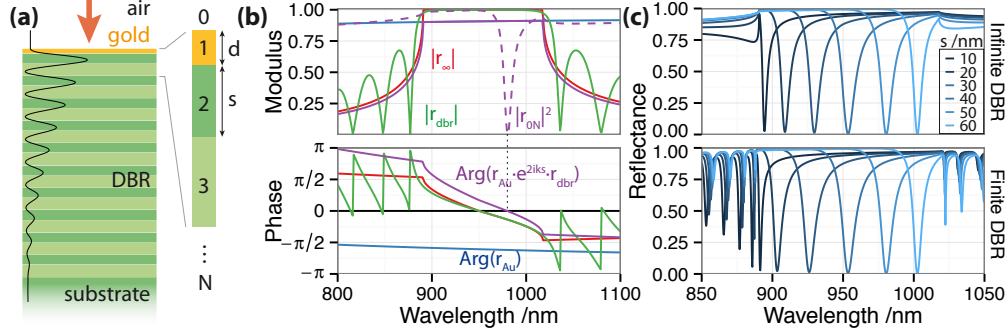


Fig. 1. (a) Schematic view of the Tamm structure; a GaAs/AlAs DBR is terminated by a thin gold film. (b) Components of the reflectivity complex variable for the Tamm structure, as described in the text. The top panel presents the modulus, the bottom panel the argument. (c) Simulated reflectivity spectra for a Tamm structure with semi-infinite DBR (top), and finite DBR (bottom) with 50 pairs of layers, varying the thickness  $s$  of the GaAs spacer adjacent to the Au metal layer from 10 nm to 60 nm.

application of the Fresnel equations at successive interfaces [23]. The multilayer is indexed from 0 to  $N$  as shown in Fig 1 (a); the reflectivity of an interface between layers (i,j) is labeled  $r_{ij}$ . Following a recursive approach, the complex reflectivity may thus be decomposed as

$$r_{0N} = \frac{r_{01} + r_{1N} \exp(2ikn_{\text{Au}}d)}{1 + r_{01}r_{1N} \exp(2ikn_{\text{Au}}d)}, \quad r_{1N} = \frac{r_{12} + r_{2N} \exp(2ikn_{\text{HS}})}{1 + r_{12}r_{2N} \exp(2ikn_{\text{HS}})}, \quad (2)$$

with  $k = 2\pi/\lambda$  the wavevector in a vacuum,  $d$  the gold thickness,  $s$  the thickness of the GaAs spacer adjacent to the metal. We seek a resonant term for the Au–DBR interface, which corresponds to the second iteration,  $r_{1N}$ . The denominator of this expression yields the resonance condition for TPs,

$$1 - r_{\text{Au}}r_{\text{DBR}} \exp(2ikn_{\text{HS}}) \approx 0, \quad (3)$$

where we identified  $r_{2N} = r_{\text{DBR}}$  with the reflection coefficient of the DBR (seen from the 2–3 interface), and  $r_{\text{Au}} = -r_{12}$  with the reflectivity of a Au–GaAs interface. This expression may also be understood as the condition of constructive round-trip for light inside the cavity formed by the first GaAs layer sandwiched between the metal and the rest of the DBR [2]. In this sense, it characterises the Tamm mode, independently of the condition of excitation, and therefore also applies to the reverse configuration where light incident from a finite DBR couples to the Tamm mode at the far end of the structure. In this case, however, coupling conditions may differ— $\Gamma_{\text{rad}}$  in particular is associated, in the view of coupled-mode theory [24], with the overlap integral between modal and incident fields, the profile of the latter being affected by the direction of incidence in the extended DBR.

Figure 1(b) illustrates the contribution of the different terms in Eq. 3, and their relation to the TP resonance. The top panel presents the modulus of the reflectivity coefficient for a bare DBR, semi-infinite (red line), and finite (50 pairs of layers, green line) with incidence from air. The characteristic stop band centred at 950 nm is clearly observed, and side-bands appear on both tails for the finite structure as a result of Fabry-Perot resonances between multiple pairs of layers [25]. The reflectivity coefficient for a Au–GaAs interface is shown in blue, with a relatively constant modulus over this spectral range. The dashed purple curve presents for comparison the full reflectance  $R_{0N} = |r_{0N}|^2$  obtained from Eq. 2, the TP mode appearing as a sharp dip at 980 nm. The bottom panel of Fig. 1(b) presents the complex argument of the same

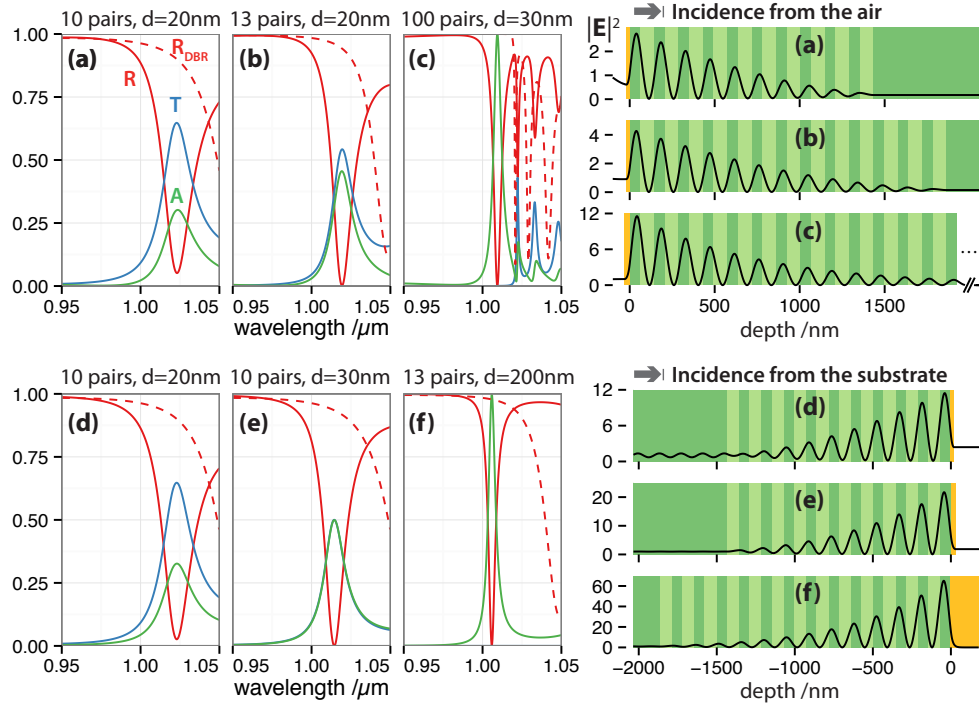


Fig. 2. Far-field response and mode profiles for different Tamm structures. Top panels consider light incident from the substrate–DBR side, while bottom panels consider the reverse situation of incidence from the air–gold side. (a, d) Unoptimised structure. (b,e) Critical coupling. (c,f) Full absorption. Note that the structure is displayed such that light always comes from the left side.

terms. The reflection coefficient for the dielectric–Au interface produces a relatively constant phase shift of about  $-\pi/2$ , while the DBR presents a linear phase shift across the stopband. The resonance condition expressed in Eq. 3 requires  $\text{Arg}(r_{\text{Au}}r_{\text{DBR}}\exp(2ikn_Hs)) = 0$ ; this zero-crossing point is observed around 980 nm, and coincides with the reflectance minimum for  $|r_{\text{ON}}|^2$  in the top panel.

A further interesting feature of TPs is the possibility of tuning the resonance position across the stopband [2], by varying the spacer thickness  $s$ , thereby affecting the phase-shift in Eq. 3. This is further illustrated in Fig. 1(c), with numerical simulations of the reflectance for a semi-infinite Tamm structure (top panel), and finite (50 pairs, bottom panel), where  $s$  was varied from 10 nm to 60 nm. We note the very close agreement in the TP resonance position and lineshape between the two models, the only noticeable difference being the appearance of side bands for the finite structure.

With these preliminary considerations in mind, we are now in a position to discuss the coupling of light to the Tamm mode, which, as we shall see, will crucially depend on the DBR parameters [20, 26], the metal thickness [9, 27, 28] and dielectric function [18, 29], as well as the direction of incidence [30, 31]. To simplify the discussion, we will restrict the study to normal incidence, the S.I. presents for completeness a simulation of the angular dispersion of the TP and its effect on critical coupling, and we refer the reader to a recent study for the relation between surface impedance and angular dispersion in perfect absorbers [32].

Figure 2 provides a global overview of the various situations under consideration. The top

panels (a,b,c) consider incidence from the air–Au side, with the leftmost panels presenting the far-field optical response (reflectance  $R$ , absorbance  $A$ , transmittance  $T$ ) at normal incidence for three different Tamm structures, while the rightmost panels show the mode profile at resonance (electric field intensity,  $|\mathbf{E}|^2$ , normalised to the incident field). Three situations are considered, (a) unoptimised structure, where light only partially couples to the Tamm mode ( $R \neq 0$ ); (b) *critical coupling* situation with  $R = 0$ ; (c) perfect absorption ( $A = 1$ ). The same layout is adopted for the bottom panels (d, e, f), where structures were selected to illustrate the reverse case of light incident from the substrate–DBR side. This allows direct comparison between the two possible experimental configurations. Note that the structure is mirrored in panels (d–f) so that light is always incident from the left side. A number of interesting features can be noted from these simulations. First, a broad range of parameters (number of layers,  $N$ , metal thickness  $d$ , spacer thickness  $s$ ) can be tuned to reach a critical coupling situation (b, c, e, f), with a different ratio of absorbance and residual transmittance. Second, the reflectivity of both mirrors (Au layer and DBR) affects the spectral position of the TP, as well as the linewidth of the mode. As the DBR (resp. Au) thickness increases, the TP mode blue-shifts and gets narrower, as a consequence of reduced radiative damping. Third, we focus on the influence of the direction of incidence on the optical response. Cases (a) and (e) are for the exact same structure, only the direction of incidence differs. The far-field properties are qualitatively similar, with a negligible shift of the TP resonance for these specific parameters. The electric field in (a) and (d) appears more strongly enhanced when light is incident from the substrate side, but this is simply a consequence of the incident irradiance (flux of the Poynting vector) scaling with the refractive index of the incident medium ( $n_1 = 3.7$  for the GaAs substrate).

The asymmetry in the response is better revealed in the different *optimised* conditions to reach critical coupling and perfect absorption. When light is incident from the air–Au side, an optimum and finite metal thickness is required to allow coupling of incident light with the Tamm plasmon mode. The DBR, however, may extend to infinity, as it prevents radiative leakage through transmission. With incidence from the DBR, on the other hand, a finite number of layers enables optimum coupling to the TP, while the metal may be optically opaque. These two different regimes for perfect absorption are further explored in the following section, with comprehensive numerical simulations.

## 2. Conditions for complete absorption

Whether light is incident from one side or the other of the Tamm structure is irrelevant for the transmission of light, following the general principle of optical reciprocity. However, the balance between absorption and reflection can be substantially affected [33]. The map of absorption shown in Fig. 3 illustrates this asymmetry with respect to the optimal number of DBR layers, and metal thickness.

Complete absorption signals a large electric field inside the metal layer, because all other layers have a purely real dielectric function. Since the Tamm mode is confined at the interface between the metal and DBR, the condition for maximum absorption coincides with a larger field enhancement in the nanostructure, with the proviso that the spatial field distribution be unaltered. Optimisation of the field enhancement is crucial to many potential applications [34], such as surface-enhanced spectroscopies [22, 30], refractive index sensing [11, 35], non-linear optics [8–10], opto-mechanical coupling [36, 37]. From the map shown in Fig. 3, we note two different conditions for complete absorption.

### 2.1. Incidence from the metal side

In this configuration, light needs to get through the metal layer to enter the structure. The field penetration into the metal layer dies off very quickly, with a typical skin depth of about 20 nm,

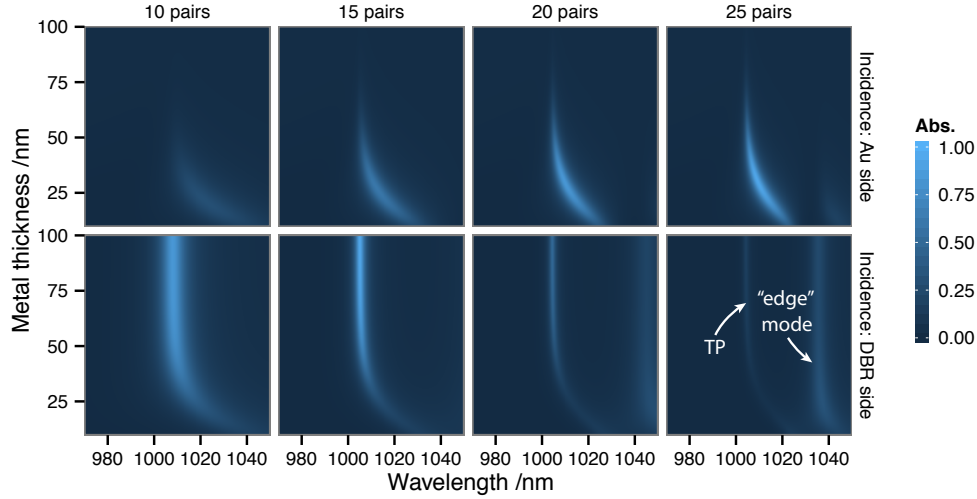


Fig. 3. Evolution of the absorbance in the region of Tamm plasmon excitation when the metal thickness is varied from 20 to 100nm. The top and bottom panels correspond to opposite direction of incident light (top: air–Au side, bottom: substrate–DBR). The number of periods in the DBR is varied in the panel columns, from 10 to 25 pairs of layers.

requiring a thin metal layer for optimal coupling (Fig. 3). The DBR should be infinite ( $>30$  pairs suffice, in practice, for these two high-contrast materials), while the metal layer has an optimum thickness of about 30 nm.

## 2.2. Incidence from the DBR side

In this case, light enters the structure from the DBR side, the metal thickness being infinite (for all practical purposes,  $>200$  nm of Au is opaque to IR light). The DBR should however have a specific number of layers, 13 pairs for this configuration, such that the in- and out-coupling of light to the Tamm mode balances precisely the Joule loss in the metal, yielding equality of radiative and non-radiative dissipation rates for the Tamm mode. Radiation leakage, responsible for  $\Gamma_{\text{rad}}$ , is directly linked to the residual transmissivity of the DBR.

To illustrate the predictive power and physical insight provided by the critical coupling argument, we isolated the radiative and non-radiative damping contributions to the TP linewidth using numerical simulations. The procedure outlined below is only strictly valid for well-defined resonances (high quality factor), as is the case for the range of parameters considered in this work. Numerical simulations were performed to calculate the far-field spectra (R, T, A) of various Tamm structures, close to the perfect absorption condition. The internal electric field intensity at a fixed position, chosen as the middle of the spacing layer, follows the same spectral profile as the far-field properties. If the gold layer is replaced by an artificial material with the imaginary part of its dielectric function set to zero, absorption cannot occur anywhere in the structure. Somewhat counter-intuitively, energy conservation dictates that the reflectance be unity across the stopband and in particular at the TP resonance (no absorption, and transmission is almost entirely blocked by the DBR), and only the internal electric field intensity signals coupling to the localised mode. The linewidth of this intensity spectrum has for only contribution the radiative loss suffered by the Tamm mode. The procedure and its results are shown in Fig. 4 for different configurations of complete absorption. In panel (a), we vary the number of

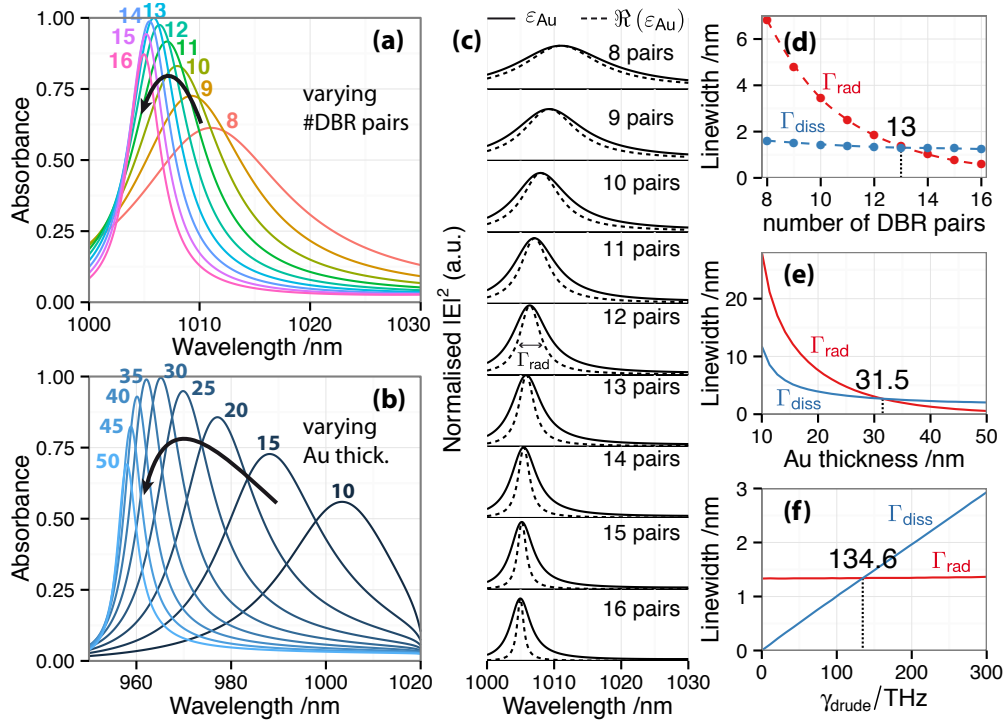


Fig. 4. Optimisation of the absorbance for the Tamm structure. (a) Illumination from the substrate, with opaque Au film. Varying the number of DBR pairs from 8 to 16, peak absorbance reaches unity for 13 pairs. (b) With incidence from the air side, and a large number of DBR pairs (50), the absorbance is optimised for a metal thickness of about 30 nm. Note that the spacing layer was slightly adjusted ( $s = 80$  nm) in order to move the TP away from the long-wavelength edge of the DBR stopband. (c) Internal field spectra for the structure in (a), presenting the electric field intensity at a fixed position (the middle of the dielectric spacer adjacent to the metal). Two simulations are presented: the metal film is made of gold (solid line), or a fictitious material for which the imaginary part of the dielectric function of gold is set to zero (dashed lines). The intensity is normalised between the two cases to facilitate the comparison of linewidths. (d-f) Evolution of the radiative ( $\Gamma_{\text{rad}}$ , red) and non-radiative ( $\Gamma_{\text{diss}}$ , blue) contributions to the total linewidth as a function of number of DBR pairs (d), metal thickness (e), and Drude scattering rate (f).



DBR pairs for a Tamm structure with opaque gold film, illuminated from the substrate. As we discussed above, the absorbance reaches unity for an optimum value of 13 pairs of layers. Panel (b) considers the opposite situation, where a semi-infinite DBR is terminated by a thin Au film (light incident from the air side). The spacer thickness was adjusted to shift the TP resonance closer to the centre of the stopband, thereby limiting the lineshape distortion above 1020 nm. Again, we observe the existence of an optimum parameter, the metal thickness, of about 30 nm. Panel (c) illustrates the procedure used to decompose the radiative and non-radiative contributions to the spectral linewidth, for the same set of parameters as in Fig. 4 (a). Two sets of simulations are presented, where the dielectric function of gold is kept as-is (solid lines), or stripped from its imaginary component (dashed lines) to remove the contribution of non-radiative damping (Joule heating,  $\Gamma_{\text{diss}} \propto \int_{\text{volume}} \Im(\epsilon) |E|^2 dV$ , with  $\Im(\epsilon)$  the imaginary part of the dielectric function). The second set of spectra (labeled  $\Re(\epsilon_{\text{Au}})$ ) was normalised to the maximum intensity for the corresponding (complex) gold simulation ( $\epsilon_{\text{Au}}$ ), to facilitate visual comparison of the linewidths. A maximum intensity is obtained for 13 pairs of layers, coinciding with the peak absorbance in panel (a), and the critical coupling condition  $\Gamma_{\text{rad}} = \Gamma_{\text{diss}}$ . This equality is further detailed in panel (d), where the two contributions  $\Gamma_{\text{rad}}$  and  $\Gamma_{\text{diss}}$  (estimated from  $\Gamma_{\text{tot}} - \Gamma_{\text{rad}}$ ) are plotted against the number of DBR pairs. Starting with 8 pairs, the resonance width is dominated by radiative damping: the DBR is too small a barrier and light over couples to the Tamm mode. Increasing the number of pairs beyond the optimum condition sees the linewidth dominated by a non-radiative component; the Tamm mode is well-confined and mostly subject to ohmic dissipation. This intrinsic loss characterises the portion of electromagnetic field localised in the metal, and varies relatively little in this range of parameters as the modal field distribution is not strongly affected by the number of pairs in the DBR. In the limit of infinite DBR, damping would be purely non-radiative, but incident light would be unable to couple to the Tamm mode. Similarly, the optimum condition observed in panel (b) matches the prediction of  $\Gamma_{\text{rad}} = \Gamma_{\text{diss}}$  highlighted in panel (e) with the optimisation of metal thickness. The interplay between radiative and non-radiative damping contributions is more subtle, as the non-radiative component is also noticeably affected by the thickness of the thin Au film, through which light must enter the structure to couple to the Tamm mode. Finally, we consider in Fig. 4 (f) the effect of the metal dielectric function itself, replacing the experimentally-obtained values for gold with a Drude model, and varying the electron-scattering rate around its measured value. As expected, the non-radiative damping contribution scales linearly with the Drude loss parameter, while the radiative contribution remains essentially constant. The condition of critical coupling reaches a consistent prediction, where  $\gamma_{\text{drude}}$  coincides with the best-fit of the Johnson and Christy data for  $\epsilon_{\text{Au}}$  (further details on the Drude model and its fit to the data are presented in the S.I.). Naturally, in the limit  $\gamma_{\text{drude}} \rightarrow 0$ , damping is purely radiative.

### 3. Tunability under critical coupling

Figure 1 illustrated that the spectral position of the Tamm mode may be tuned by varying the thickness of the dielectric spacer immediately adjacent to the metal. In this concluding section, we discuss the conditions under which such tuning may preserve the critical coupling condition.

A marked contrast is observed in Fig. 5 for the two configurations: light incident from the substrate with a finite DBR, (a); light incident from the air side with a thin Au film, (b). In Fig. 5 (a) the thickness of the spacer has a strong detrimental effect on critical coupling. How can we understand this difference with the opposite configuration shown in Fig. 1(c) and repeated in Fig. 5 (b), where tuning of the TP over a wide spectral range can be obtained while maintaining the critical coupling (and perfect absorbance condition)? We use an analogy with the process of critical coupling to surface plasmon-polaritons (SPPs) described in Ref. [15] to interpret this behaviour. In the Kretschmann (or Otto) configuration, light couples to propagating SPPs via

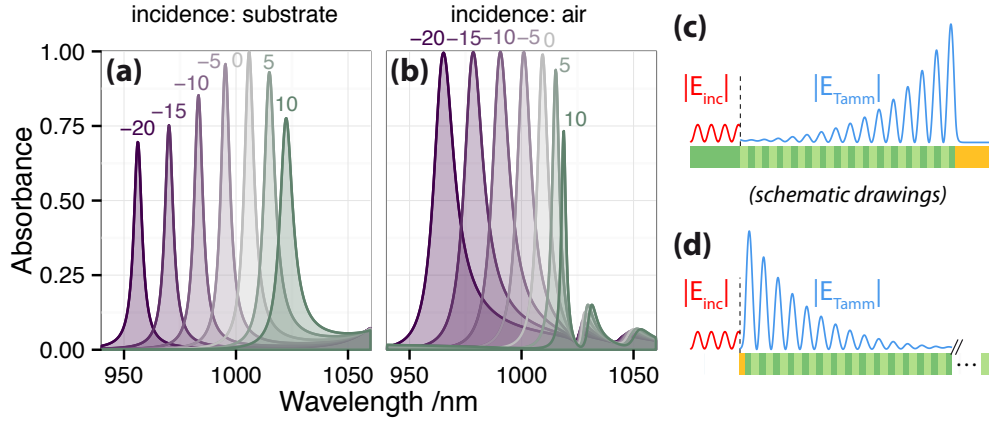


Fig. 5. Tunability of the TP resonance and its effect on critical coupling. (a) Absorbance spectra for a Tamm structure with finite DBR and opaque gold film, with light incident from the substrate side. The spacer layer thickness is varied around its nominal thickness  $\lambda/4 \approx 64$  nm from in the range  $[-20; +10]$  nm. Only the nominal thickness presents complete absorbance. (b) Absorbance spectra corresponding to a practically semi-infinite DBR structure (50 pairs) terminated by a 30 nm-thin Au film, with incidence from the air side. The spacer thickness variation shifts the Tamm resonance across the stopband, while maintaining unit absorbance. (c) and (d) Schematic drawings of the spatial distribution of the Tamm modal field relative to the incident field (shown with arbitrary phase), in both configurations.

attenuated total internal reflection, and the observed drop in reflectivity can be interpreted as a quantum interference between two indistinguishable pathways: i) total internal reflection, ii) conversion of light to SPPs, followed by re-radiation in the prism (radiative decay). For the Tamm structure depicted in the schematics of Fig. 5(c, d) the two interfering pathways would be i) direct reflection from the first mirror (DBR for Fig. 5(c), Au for Fig. 5(d)); ii) conversion to TPs, followed by re-radiation (with probability proportional to  $\Gamma_{rad}$ ). Naturally, the condition of critical coupling requires an exact match of amplitude and phase between the two pathways. We note at this point that the modal field associated with Tamm plasmons is remarkably insensitive to a small variation of the spacer thickness (further simulations are shown in the S.I.). Thus, when light enters the structure from the air-Au side, a constant phase relationship is maintained between the incident light and the Tamm mode. In contrast, with incidence from the substrate-DBR side, the tail of the Tamm mode which couples to free radiation undergoes an important phase shift as the first DBR interface is displaced with the spacer thickness (Fig. 5 c).

In order to maintain a condition of optimal coupling, the DBR structure in Fig. 5 (a, c) should undergo concomitant changes in the number of layers together with the spacer variation. In other words, a specific number of layers only allows a limited range of tunability of the critically-coupled TP mode for this direction of incidence.

#### 4. Conclusions

We have presented and explained conditions for optimised coupling between light and Tamm plasmons excited at normal incidence from either side of the Au-DBR structure, using the powerful concept of critical coupling. With comprehensive numerical simulations, we elucidated the asymmetry in reflection and absorption with respect to the direction of incident light, and found parameters that yield complete absorption in both configurations. The signature of

critical coupling was confirmed in the equality of absorptive and radiative dissipation rates. These physical insights may be used in the design of optimised narrow-band tunable absorbers and thermal emitters.

### **Acknowledgments**

B.A. wishes to thank Jean-Jacques Greffet and Christophe Sauvan for fruitful discussions at the Institut d'Optique in Orsay.